Fractal properties of robust strange nonchaotic attractors in maps of two or more dimensions

Jong-Won Kim,[1] Sang-Yoon Kim,[2,*] Brian Hunt,[3] and Edward Ott[1,4]
[1]*Institute for Research in Electronics and Applied Physics, and Department of Physics, University of Maryland, College Park, Maryland 20742*
[2]*Institute for Research in Electronics and Applied Physics, University of Maryland, College Park, Maryland 20742*
[3]*Institute for Physical Science and Technology, and Department of Mathematics, University of Maryland, College Park, Maryland 20742*
[4]*Department of Electrical and Computer Engineering, University of Maryland, College Park, Maryland 20742*
(Received 16 September 2002; published 26 March 2003)

We consider the existence of robust strange nonchaotic attractors in a simple class of quasiperiodically forced systems. Rigorous results are presented demonstrating that the resulting attractors are strange in the sense that their box-counting dimension D_0 is larger than their information dimension D_1 by 1 (i.e., $D_0 = D_1 + 1$). We also show how this property is manifested in numerical experiments.

DOI: 10.1103/PhysRevE.67.036211 PACS number(s): 05.45.Df, 05.45.Ac, 05.45.Pq

I. INTRODUCTION

The phrase *strange nonchaotic attractor* (SNA) [1] refers to an attractor that is nonchaotic in the sense that its orbits are not exponentially sensitive to perturbation (i.e., none of the Lyapunov exponents are positive), but the attractor is strange in the sense that its phase space structure has nontrivial fractal properties. Past studies indicate that SNA's are *typical* in nonlinear dynamical systems that are quasiperiodically forced. Here by a typical behavior we mean that the behavior occurs for a positive measure set of parameter values. Alternatively, if parameters are chosen at random from an ensemble with a smooth probability density, then the probability of choosing parameters that yield a typical behavior is not zero. The description of a behavior as typical is to be contrasted with the stronger statement that a behavior is *robust*. In particular, we say that the behavior of a system is robust if it persists under sufficiently small perturbations; i.e., there exist a positive value δ such that the robust behavior occurs for all systems that can be obtained by perturbation of the original system by an amount less than δ. Thus all robust behaviors are also typical, but not vice versa.

With respect to SNA's, examples where they are typical but not robust have been extensively studied [2–5]. An example of this type is the quasiperiodically forced circle map given by the system [3]

$$\theta_{n+1} = [\theta_n + \omega] (\mathrm{mod} 2\pi), \tag{1a}$$

$$\varphi_{n+1} = [\varphi_n + \omega_\varphi + \varepsilon \sin \varphi_n + C \cos \theta_n] (\mathrm{mod} 2\pi), \tag{1b}$$

where $\Omega \equiv \omega/2\pi$ is irrational. Other examples of typical nonrobust SNA's involving differential equations have also been studied [2,4]. Numerical evidence [3,4] and analysis based on a correspondence [2,5] with Anderson localization in a quasiperiodic potential leads to an understanding of the typical but nonrobust nature of SNA's in these examples: In particular, it is found that SNA's exist on a positive Lebesgue measure Cantor set in parameter space. In the case of Eq. (1), for example, consider the rotation number

$$W = \lim_{n \to \infty} (\varphi_n - \varphi_0)/(2\pi n), \tag{2}$$

where for this limit, φ_n is *not* computed modulo 2π. For fixed ω, $\varepsilon > 0$, and $C > 0$, a plot of W versus ω_φ yields an incomplete devil's staircase, a nondecreasing graph consisting of intervals of ω_φ, where $W(\omega_\varphi)$ is constant and with the increase of $W(\omega_\varphi)$ occurring only on a Cantor set of positive measure. For small ε, the values of ω_φ on the Cantor set correspond to orbits that are three frequencies quasiperiodic, but for larger ε they correspond to SNA's. Because an arbitrarily small perturbation of ω_φ from a value in the Cantor set can result in a value of ω_φ outside the Cantor set, these SNA's are not robust. On the other hand, because the Cantor set of ω_φ values has a positive Lebesgue measure (''positive length''), these attractors are typical for Eq. (1).

Other studies suggest that there are situations where SNA's are robust [1,6–12]. The experiment of Ditto *et al.* [6] on a quasiperiodically forced magnetoelastic ribbon produced evidence of a SNA, and the existence of this SNA appeared to be stable to parameter perturbations. The original paper where the existence of SNA's in quasiperiodically forced systems was first discussed [1] gives numerical evidence of robust SNA's. In addition, the effect of quasiperiodic perturbations on a system undergoing a periodic doubling cascade has been investigated, and evidence has been presented suggesting that, after a finite number of torus doublings, a robust SNA results [7,9].

Thus there seem to be two types of SNA's: typical, nonrobust SNA's, and robust SNA's. In this paper we study a class of models exhibiting robust SNA's. The model class that we study is particularly interesting because it allows the possibility of rigorous analysis. In particular, we are able to prove, under the mild hypothesis that a certain Lyapunov exponent is negative, that the attractor is strange and nonchaotic. Since other cases of SNA's are likely to be accessible only to study by numerical means, it is worthwhile to investigate our, more well-understood models numerically. By doing this we gain insight into the applicability and limitations of numerical techniques for the study of SNA's.

*Permanent address: Department of Physics, Kangwon National University, Chunchon, Kangwon-Do 200-701, Korea.

In this paper we consider quasiperiodically forced maps, which can be motivated by the consideration of a system of ordinary differential equations in the form $d\mathbf{x}/dt = \mathbf{F}(\mathbf{x}, \xi, \theta^{(1)}, \theta^{(2)}, \ldots, \theta^{(N)})$, where $\mathbf{F}$ is 2π periodic in the angles ξ and $\theta^{(i)}$, which are given by $\xi = \omega_\xi t + \xi_0$ and $\theta^{(i)} = \omega_{\theta^{(i)}} t + \theta_0^{(i)}$, and $\omega_\xi, \omega_{\theta^{(1)}}, \ldots, \omega_{\theta^{(N)}}$ are incommensurate. Sampling the state of the system at discrete times t_n given by $\xi = 2n\pi$, we obtain a mapping of the form

$$\theta_{n+1}^{(i)} = [\theta_n^{(i)} + \omega^{(i)}] (\mathrm{mod} 2\pi), \tag{3a}$$

$$\mathbf{x}_{n+1} = \tilde{\mathbf{F}}(\mathbf{x}_n, \theta_n^{(1)}, \theta_n^{(2)}, \ldots, \theta_n^{(N)}), \tag{3b}$$

where $\mathbf{x}_n = \mathbf{x}(t_n)$, $\omega^{(i)} = 2\pi\omega_{\theta^{(i)}}/\omega_\xi$, and there exist no set of integers $(m^{(0)}, m^{(1)}, \ldots, m^{(N)})$ for which $\sum_{i=1}^N m^{(i)}\omega^{(i)} = 2\pi m^{(0)}$, aside from $(m^{(0)}, m^{(1)}, \ldots, m^{(N)}) = (0,0,\ldots,0)$.

For the map (3), the simplest possible attractor is an N-dimensional torus, $\mathbf{x} = \mathbf{f}(\theta^{(1)}, \theta^{(2)}, \ldots, \theta^{(N)})$. In this paper, we consider the case where an attracting $(N+1)$-dimensional torus exists, and the dynamics on the torus is given by

$$\theta_{n+1}^{(i)} = [\theta_n^{(i)} + \omega^{(i)}] (\mathrm{mod} 2\pi), \tag{4a}$$

$$\varphi_{n+1} = [\varphi_n + q^{(1)}\theta_n^{(1)} + q^{(2)}\theta_n^{(2)} + \ldots + q^{(N)}\theta_n^{(N)} + P(\varphi_n, \theta_n^{(1)}, \theta_n^{(2)}, \ldots, \theta_n^{(N)})] (\mathrm{mod} 2\pi), \tag{4b}$$

where P is periodic in all its variables and $q^{(1)}$, $q^{(2)}, \ldots, q^{(N)}$ are integers. We are particularly interested in the case in which Eq. (4b) is invertible, so that no chaos is possible, and when at least one $q^{(i)}$ is nonzero, which as we will see prevents the existence of an attracting N-torus.

In Sec. II we examine the simplest case where $N=1$ $(\theta^{(i)} \to \theta)$. Section II A presents numerical experiments and rigorous analysis of this two-dimensional map model. In particular, we prove (subject to a mild hypothesis on the negativity of a Lyapunov exponent) that, for our class of maps, the information dimension of the SNA is 1 $(D_1 = 1)$, while its box-counting dimension is 2 $(D_0 = 2)$ [13]. Thus we rigorously characterize the nature of the strangeness of the SNA's for our model. [In a previous work [14] it was argued (nonrigorously) that $D_1 = 1$ and $D_0 = 2$ for the two-dimensional SNA map introduced in Ref. [1].] We conjecture that $D_1 = 1$ and $D_0 = 2$ *typically holds for SNA's of two-dimensional quasiperiodically forced maps* [i.e., maps of the form $\theta_{n+1} = (\theta_n + \omega) \mathrm{mod} 2\pi$, $\varphi_{n+1} = F(\varphi_n, \theta_n)$ with $\Omega \equiv \omega/2\pi$ irrational]. Also, in Sec. II A we present numerical experiments on dimension calculations of D_1 and D_0, and of the Lyapunov exponent for our map. Section II B investigates the dynamical origin of SNA's as a limit as Ω approaches its irrational value through an infinite sequence of finer and finer rational approximations [15]. It turns out that this technique yields substantial insight into the structure of SNA's, as well as additional understanding of why $D_1 = 1$ and $D_0 = 2$ applies.

Section III considers higher-dimensional maps. In particular, Sec. III A considers the case where $\mathbf{x}$ in Eq. (3b) is two dimensional and $N=1$, while Sec. III B considers $N>1$ with $\mathbf{x}$ being a scalar angle variable (as in Sec. II). For the map of Sec. III A, we consider one component of $\mathbf{x}$ to be an angle variable and the other component to be analogous to a radial variable. Thus, if, on the attractor, the radial coordinate depends smoothly on the other two variables (which are angles), then the attractor lies on a two-torus, and the considerations of Sec. II apply directly. On the other hand, the existence of such a smooth two-torus is in question, and this is the main issue addressed in Sec. III A. For the map of Sec. III B we are able to generalize the rigorous approach of Sec. II A to show that for this class of maps $D_0 = N+1$, while $D_1 = N$. In addition, numerical experiments are performed to test the convergence of dimension computations to these values.

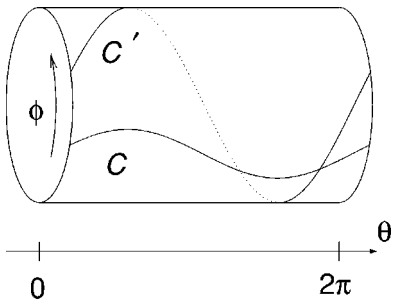

FIG. 1. Torus unwrapped in the θ direction ($\theta = 0$ and $\theta = 2\pi$ are identified with each other). The map (5) takes the curve C to the curve C'.

II. TWO-DIMENSIONAL MAP ON A TORUS

A. Existence of SNA

We investigate the simplest case of Eq. (3) where $N=1$ $(\theta^{(i)} \to \theta)$ and the state variable $\mathbf{x}$ is one dimensional. Specifically, we take $\mathbf{x}$ to be an angle variable φ, so that the map operates on a two-dimensional θ-φ torus. Within this class we restrict consideration to maps of the form

$$\theta_{n+1} = [\theta_n + \omega] (\mathrm{mod} 2\pi), \tag{5a}$$

$$\varphi_{n+1} = [\theta_n + \varphi_n + \eta P(\theta_n, \varphi_n)] (\mathrm{mod} 2\pi), \tag{5b}$$

where $\omega = \pi(\sqrt{5} - 1)$, and $P(\theta, \varphi)$ is continuous, differentiable, and 2π periodic in both of its arguments (θ and φ). When η is small enough ($|\eta| < \eta_c$), this map is invertible. That is, the map is solvable for (θ_n, φ_n) when $(\theta_{n+1}, \varphi_{n+1})$ is given. We choose a simple function $P(\theta, \varphi) = \sin\varphi$ for our numerical work. In this case, the system is invertible if $|\eta| < 1$. Furthermore, since the map is invariant under the change of $\eta \to -\eta$ and $\varphi \to \varphi + \pi$, it is sufficient to consider only the case $\eta \geqslant 0$.

Figure 1 illustrates how a curve C on the θ-φ toroidal surface is mapped to a curve C' by the map (5). Note that the torus is unrolled in the θ direction to visualize the whole curve C in a two-dimensional surface, but still rolled in the φ direction. The curve C circles around the torus in the θ direction, but does not wrap around the torus in the φ direction. After one iterate of Eq. (5), the curve C is mapped to a

curve C' that wraps once around the torus in the φ direction. This behavior comes about due to the term θ_n on the right-hand side of Eq. (5b), because $\theta+\varphi+\eta P(\theta,\varphi)$ increases by 2π as θ increases by 2π. Similarly, applying the map to C' produces a curve with two wraps around the torus in the φ direction, and so on.

The main results of our numerical experiments and rigorous analysis of Eq. (5) with $|\eta|<\eta_c$ are as follows.

(i) The map (5) has a single attractor.

(ii) For typical $P(\theta,\varphi)$, the attractor has a Lyapunov exponent h_φ that is negative for $\eta\neq 0$.

(iii) The attractor has information dimension 1 for $\eta\neq 0$.

(iv) The attractor is the entire θ-φ torus and, hence, has a box-counting dimension 2.

(v) These results are stable to the perturbations of the system.

We first establish (ii) using an approximate formula for h_φ for small η. Our evidence for (ii) is strong but a rigorous mathematical proof is lacking. If we adopt (ii) as a hypothesis, then all the other results rigorously follow.

Lyapunov exponent. A trajectory of the map (5) has two Lyapunov exponents h_θ and h_φ, where $h_\theta=0$ is associated with Eq. (5a) and h_φ is associated with Eq. (5b). The latter exponent is given by the formula

$$h_\varphi=\int \ln[1+\eta P_\varphi(\theta,\varphi)]d\mu, \tag{6}$$

where $P_\varphi=\partial P/\partial\varphi$, and μ denotes the measure generated by the orbit from a given initial point $(\theta_0,\ \varphi_0)$.

If $h_\varphi>0$ for a particular trajectory, then, since $h_\theta=0$, the map exponentially expands areas near the trajectory in the limit $n\to\infty$. Since the θ-φ torus has a finite area, if the map is invertible, then there cannot be a set of initial points of nonzero area (positive Lebesgue measure) for which $h_\varphi>0$, and the map thus does not have a chaotic attractor. Thus $h_\varphi\leqslant 0$ for typical orbits.

Furthermore, we argue that $h_\varphi<0$ for small nonzero η. We consider first the case $\eta=0$, for which Eq. (5b) becomes $\varphi_{n+1}=(\theta_n+\varphi_n)(\mathrm{mod}2\pi)$. If we initialize a uniform distribution of orbit points in the θ-φ torus, then, on one application of the $\eta=0$ map, the distribution remains uniform. Furthermore, this uniform distribution is generated by the orbit from any initial condition. To verify this, we note that the explicit form of an $\eta=0$ orbit, $\theta_n=(\theta_0+n\omega)(\mathrm{mod}2\pi)$, $\varphi_n=[\varphi_0+n\theta_0+\frac{1}{2}(n^2-n)\omega](\mathrm{mod}2\pi)$, is shown to generate a uniform density in Ref. [16]. We can obtain an approximation to h_φ for nonzero but small η by expanding $\ln(1+\eta P_\varphi)$ in Eq. (6) to order η^2 and assuming that, to this order, the deviation of the measure μ from uniformity is not significant $[d\mu\approx d\theta d\varphi/(2\pi)^2]$. Using $\ln(1+\eta P_\varphi)=\eta P_\varphi-(1/2)\eta^2P_\varphi^2+O(\eta^3)$, this gives

$$h_\varphi=-\frac{1}{2}\eta^2\langle P_\varphi^2\rangle+o(\eta^2), \tag{7}$$

which is negative for small enough $\eta\neq 0$. Here $\langle P_\varphi^2\rangle$ denotes the θ-φ average of P_φ^2, and the order η term is absent by virtue of $\int_0^{2\pi}P_\varphi d\varphi=0$. Since we cannot show the convergence of an expansion in η, our result (7) is formal rather than rigorous. However, numerical results strongly support Eq. (7). Figure 2 shows a plot of h_φ versus η for $P(\theta,\varphi)=\sin\varphi$. Remarkably, Eq. (7) (the straight line) describes the numerical data to better than 8% even for η as large as 0.5.

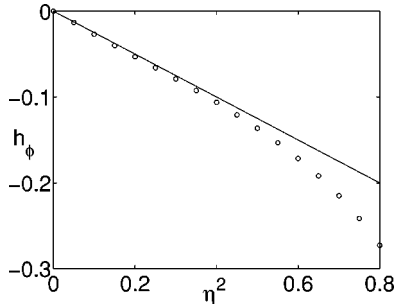

FIG. 2. Lyapunov exponent h_φ vs η^2. For each η, the data plotted as open circles were computed from 10^7 iterations of the map (5) with $\omega=\pi(\sqrt{5}-1)$ and $P(\theta,\varphi)=\sin\varphi$.

Dimensions of the SNA. For our map, the information dimension cannot be less than 1 due to the quasiperiodic θ dynamics. In addition, the Lyapunov dimension is an upper bound of information dimension [17]. Therefore, if we accept (ii), $h_\varphi<0$, then $h_\theta=0$ implies (iii).

Results (iii) and (iv) quantify the strangeness of the attractor. In particular, since the information dimension of the attractor is 1, orbits spend most of their time on a curvelike set; yet, since the box-counting dimension is 2, if one waits long enough, a typical orbit eventually visits any neighborhood on the θ-φ torus. One can get a sense of this result from the numerical orbit shown in Fig. 3, in which a trajectory of length 10^4 appears to be concentrated along one-dimensional strands [Fig. 3(a)], but for the same parameters a trajectory of length 10^5 fills much more of the θ-φ torus [Fig. 3(b)].

We show in Fig. 4(a) a plot of $\log_2N(\varepsilon)$ versus $\log_2(1/\varepsilon)$, and in Fig. 4(b) a plot of $\Sigma p_i\log_2(1/p_i)$ versus $\log_2(1/\varepsilon)$. Here $N(\varepsilon)$ is the number of $\varepsilon\times\varepsilon$ boxes (in θ-φ space) needed to cover the points from an orbit of length T, and p_i is the fraction of those orbit points in the ith $\varepsilon\times\varepsilon$ box. According to our previous arguments on dimensions, in the limit $T\to\infty$, the points in Figs. 4(a) and 4(b) should follow a straight line of slope 2 and 1 for small ε, corresponding to a box-counting dimension of 2 and an information dimension

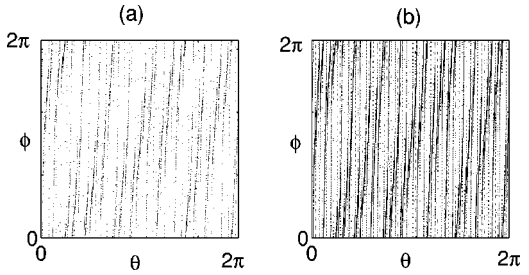

FIG. 3. Trajectory of the map (5) with $\omega=\pi(\sqrt{5}-1)$, $\eta=0.3$, and $P(\theta,\varphi)=\sin\varphi$. In each case $\theta_0=\varphi_0=0$, and 10^4 points of the trajectory are computed before plotting; in (a) the next 10^4 points are plotted, while (b) shows 10^5 points.

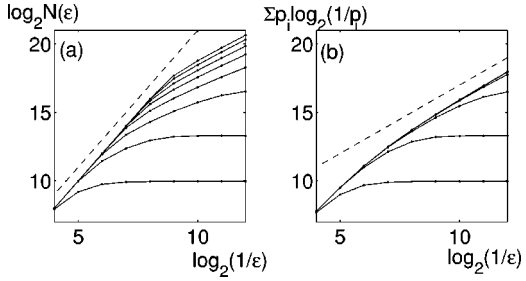

FIG. 4. Dimension computations for Eq. (5) with $\eta=0.3$, $\omega=\pi(\sqrt{5}-1)$, and $P(\theta,\varphi)=\sin\varphi$. In (a) the dashed line has slope 2, while in (b) it has slope 1. In each graph, the curves from lowest to highest represent $T=10^3,10^4,\ldots,10^{10}$; in (b) the final five curves are virtually identical.

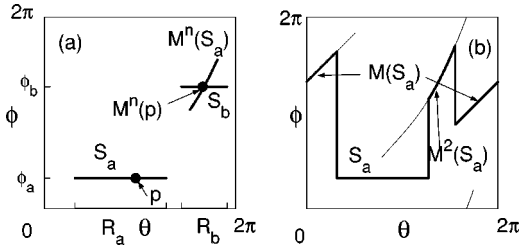

FIG. 5. (a) The nth iterate of S_a intersects S_b. The nth preiterate of this intersection point (denoted p) is a point on S_a that goes to S_b in n iterates. (b) S_a plus its first two iterates, $M(S_a)$ and $M^2(S_a)$, cover the entire 2π range of θ. $M(S_a)$ and $M^2(S_a)$ are shown as thin lines. The curve G_a, which includes S_a, pieces of $M(S_a)$ and $M^2(S_a)$, and vertical segments connecting these pieces, is shown as a dark thick line.

of 1. As is commonly found, the box-counting dimension computation converge rather slowly with increasing orbit length T. Thus, we show plots in Fig. 4 for several different T. As can be seen in Fig. 4(a), the ε range consistent with a slope of 2 (the straight line in the figure) steadily increases toward smaller ε [larger $\log_2(1/\varepsilon)$] as T increases. This is in contrast with Fig. 4(b), which appears to reach a form independent of T that is consistent with a small ε slope of 1. While the convergence in Figs. 4(a) and 4(b) is consistent with box-counting and information dimensions of 2 and 1, the slowness of the convergence also indicates that a purely numerical determination of the dimension values is suspect.

Topological transitivity. To establish results (i) and (iv), that the attractor of the map is in the whole θ-φ torus, we prove that the map is *topologically transitive*: For every pair of open disks A and B, there is a trajectory that starts in A and passes through B. This property is known to imply that a dense set of initial conditions yields trajectories each of which is dense in the torus [18]. In particular, any attractor having an open basin of attraction must contain a dense orbit, and, hence, must be the entire torus.

Let M be the map (5). We will show in fact that for every pair of line segments $S_a=\{(\theta,\varphi):\theta\in R_a \text{ and } \varphi=\varphi_a\}$ and $S_b=\{(\theta,\varphi):\theta\in R_b \text{ and } \varphi=\varphi_b\}$, where $R_a=(\theta_a,\theta_a+\delta_a)$ and $R_b=(\theta_b,\theta_b+\delta_b)$, there is a finite trajectory of M that begins on the first segment and ends on the second. (Choosing S_a to lie in A and S_b to lie in B, this implies topological transitivity.) In other words, we will show that the nth iterate of S_a intersects S_b for some positive integer n; see Fig. 5(a). Our strategy is to iterate S_a forward until the union of its iterates covers all values of θ at least once; the number of iterates needed is finite and depends only on δ_a. By selecting pieces of these iterates that cover each value of θ exactly once, we form the graph $\varphi=g_a(\theta)$ of a piecewise continuous function g_a; see Fig. 5(b). Similarly we form a graph $\varphi=g_b(\theta)$ from pieces of backward iterates of S_b. Finally, we show that some forward iterate of the graph of g_a must intersect the graph of g_b.

The following is a formal definition of g_a. Let M_θ be the map (5a). For each θ, let $k(\theta)$ be the smallest non-negative integer for which $\theta\in M_\theta^{k(\theta)}(R_a)$. [In Fig. 5(b), $k(\theta)=0$, 1, or 2 for all θ.] Let $g_a(\theta)$ be the φ coordinate of the $k(\theta)$th iterate under M of $(M_\theta^{-k(\theta)},\varphi)\in S_a$. Then the graph $\varphi=g_a(\theta)$ has a finite number d_a of discontinuities. Each contiguous piece of this graph is a forward iterate of some piece of S_a.

Now form the curve G_a by taking the graph of g_a and adding line segments in the φ direction at each value of θ where g_a is discontinuous. (We take these segments to lie in $0<\varphi<2\pi$.) Thus we make G_a a contiguous curve. See Fig. 5(b), which illustrates this construction for a case where $d_a=3$. Notice that, for each n, the nth iterate of G_a is also a contiguous curve that consists of the graph of a function with d_a discontinuities, together with d_a "connecting segments." Define g_b and G_b similarly to g_a and G_a, but in terms of the backward iterates of the S_b. Let d_b be the number of discontinuities of g_b.

Our goal is to show that for n sufficiently large, $M^n(G_a)$ intersects G_b for at least d_a+d_b+1 different values of θ. Then since there are at most d_a+d_b values of θ at which one of these two curves has a connecting segment, there will be at least one intersection point between the nth iterate of the graph of g_a and the graph of g_b. Since the graph of g_a consists of forward iterates of S_a and the graph of g_b consists of backward iterates of S_b, some forward iterate of S_a will intersect S_b, as we claimed.

As noted before (see Fig. 1), each successive iteration $M^n(G_a)$ "wraps around" the torus in the φ direction once more than the prior iteration $M^{n-1}(G_a)$. The number of wraps of such a curve is more formally called the "winding number" of the curve, and may be any integer (possibly negative). For example, in Fig. 5(b) the winding number of G_a is 0. As n increases, the winding number of $M^n(G_a)$ will eventually exceed the winding number of G_b by at least d_a+d_b+1. Hence $M^n(G_a)$ intersects G_b for at least d_a+d_b+1 different values of θ as desired. This establishes claims (i) and (iv).

Notice that the argument above does not depend on the specific form of $P(\theta,\phi)$, only that it is continuous and periodic and that η is sufficiently small ($|\eta|<\eta_c$), so that the map (5) is one-to-one. This independence of the results from the specific form of $P(\theta,\phi)$ implies that the results are stable to system changes [our claim (v)] that preserve a quasiperiodic driving component (5a).

Discussion. The possible existence of SNA's was origi-

nally pointed out in Ref. [1], and many numerical explorations of the dynamics on attractors that are apparently strange and nonchaotic have appeared. Recently, there has also been rigorous results on the mathematical properties that SNA's must have if they exist [19]. In spite of these works, a very basic question has remained unanswered: *Can it be rigorously established that SNA's generically exist in typical quasiperiodically forced systems?* This is an important issue, because, although the numerical evidence for SNA's is very strong, perhaps the attractors observed are nonstrange with a very fine scale structure (rather than the *infinitesimally* fine scale structure of a truly strange attractor). Also, there might be the worry that the numerical evidence is somehow an artifact of computational error. Our proof of topological transitivity, combined with the hypothesis that $h_{\varphi}<0$, answers the question of the typical existence of SNA's (affirmatively) (Ref. [13] contains a preliminary report of our work). The only previous work rigorously establishing the existence of a SNA is that appearing in the original publication on SNA's [1] and in Ref. [20]. These proofs, however, are for a very special class of quasiperiodically forced system such that an arbitrarily small typical change of the system puts it out of the class. Thus this proof does not establish that SNA's exist in typical quasiperiodically forced situations. In order to see that nature of this situation with respect to Refs. [1,20], we recall the example treated in Ref. [1]. In that reference the map considered was $x_{n+1}=2\lambda(\tanh x_n)\cos\theta_n \equiv f(x_n,\theta_n)$, with θ_n evolving as in Eq. (5a). It was proven in Ref. [1] that this map has a SNA for $\lambda>1$. However, the map has an invariant set, namely, the line $x=0$, θ in $[0,2\pi)$, and this fact is essential in the proof of Ref. [1]. On the other hand, the existence of this invariant set does not persist under perturbations of the map. Thus, if we perturb $f(x,\theta)$ to $f(x,\theta)+\varepsilon g(x,\theta)$, the invariant set is destroyed, even for small ε, for any typical function $g(x,\theta)$ [in particular, an arbitrarily chosen $g(x,\theta)$ is not expected to satisfy $g(0,\theta)=0$].

B. Origin of SNA's: Rational approximation

Using rational approximations (RA's) to the quasiperiodic forcing, we now investigate the origin for the appearance of SNA's in Eq. (5) for $P(\theta,\varphi)=\sin\varphi$ and $\omega=\pi(\sqrt{5}-1)$. For the case of the inverse golden mean $\Omega\equiv\omega/2\pi$, its rational approximants are given by the ratios of the Fibonacci numbers, $\Omega_k=F_{k-1}/F_k$, where the sequence of $\{F_k\}$ satisfies $F_{k+1}=F_k+F_{k-1}$ with $F_0=0$ and $F_1=1$. Instead of the quasiperiodically forced system, we study an infinite sequence of periodically forced systems with rational driving frequencies Ω_k. We suppose that the properties of the original system may be obtained by taking the quasiperiodic limit $k\to\infty$.

For each RA of level k, a periodically forced map with the rational driving frequency Ω_k has a periodic or quasiperiodic attractor that depends on the initial phase θ_0 of the external force. Then we take the union of all attractors for different θ_0 to be the kth RA to the attractor in the quasiperiodically forced system. Furthermore, due to the periodicity, it is sufficient to obtain the RA by changing θ_0 only in a basic interval $\theta_0\in[0,1/F_k)$, because the RA to the attractor in the remaining range, $[1/F_k,1)$, may be obtained through (F_k-1) iterations of the result in $[0,1/F_k)$. For a given k we call the periodic attractors of period F_k the ''main periodic component.'' The first column of Fig. 6 shows that the Lebesgue measure of the main periodic component (denoted by the solid line) becomes dominant as the level k increases (i.e., the fraction of the θ axis corresponding to the nonperiodic, gray area decreases). By iterating the RA in the basic interval of θ, we obtain the RA in the whole range of θ, as shown in the second column of Fig. 6. As k increases, the whole RA becomes more similar to its quasiperiodic limit given in Fig. 3.

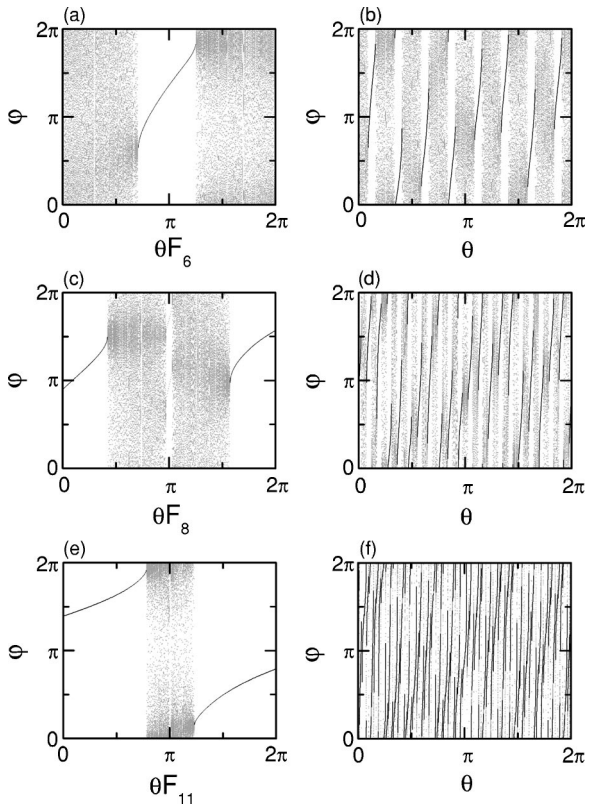

FIG. 6. RA's for $\eta=0.3$. The levels are $k=6$ in (a) and (b), $k=8$ in (c) and (d), and $k=11$ in (e) and (f). In the first column the RA in the basic interval of θ is given, while in the second column the RA in the whole range of θ is given. The quasiperiodic component is represented in gray dots and the main periodic component is denoted by the solid line.

We first note that for $\eta=0$ the RA to the regular quasiperiodic attractor consists of only the quasiperiodic component. However, as η becomes positive, periodic components appear via phase-dependent (i.e., θ_0-dependent) saddle-node bifurcations. As examples, see the first column of Fig. 6. Here the quasiperiodic component is plotted in the gray. ''Gaps'' in the gray quasiperiodic components are occupied by the main periodic components (denoted by solid lines) with period F_k and the minor periodic components with higher period mF_k $(m=2,3,4,\ldots)$. Figures 7(a) and 7(b) show the saddle-node bifurcation curves in the θF_k-η plane, at which the main periodic components with period F_k are born. It can be easily seen that for a given η, the width of the main gap (occupied by a period-F_k attractor) becomes larger

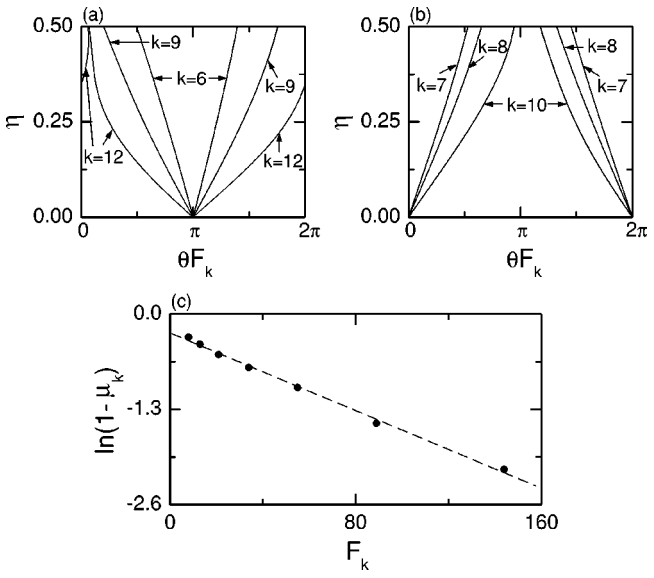

FIG. 7. Phase-dependent saddle-node bifurcation lines for the main periodic components. The cases of the level $k=6,9,12$ are shown in (a), and other cases with $k=7,8,10$ are given in (b). (c) Plot of $\ln(1-\mu_k)$ vs F_k for $\eta=0.3$. Solid points denote the data for levels $k=6,\ldots,12$, which are well fitted with a dashed straight line with slope $\alpha=0.013$.

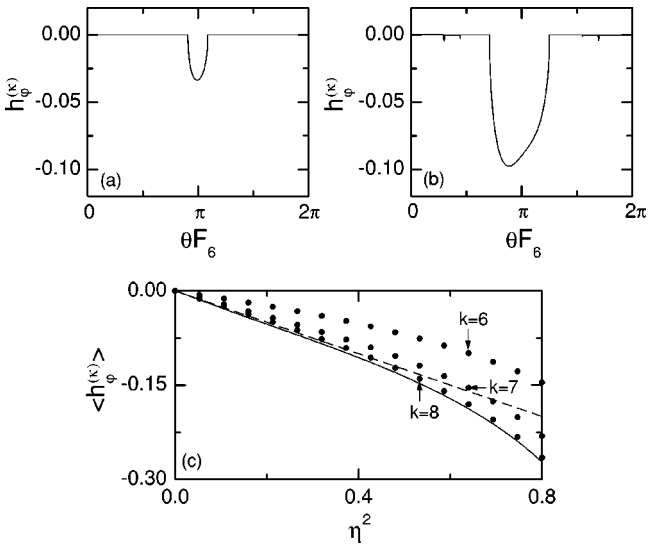

FIG. 8. Plot of $h_\varphi^{(k)}(\theta)$ vs θF_6 for (a) $\eta=0.1$ and (b) $\eta=0.3$. (c) Plot of $\langle h_\varphi^{(k)}\rangle$ vs η^2 for the three levels $k=6$, 7, and 8. The solid and dashed lines denote the Lyapunov exponents in the quasiperiodic limit that are obtained numerically and analytically, respectively.

as k increases. Quantitatively, it is found that the Lebesgue measure μ_k in θ for the main periodic component becomes dominant as k increases; i.e., the Lebesgue measure $(1-\mu_k)$ of the complementary set decreases exponentially with F_k; $(1-\mu_k)\sim e^{-\alpha F_k}$, where $\alpha=0.013$, as shown in Fig. 7(c) for $\eta=0.3$.

In what follows, we use the RA's to explain the origin of the negative Lyapunov exponent h_φ and the strangeness of the SNA. For a given level k of the RA, let $h_\varphi^{(k)}(\theta)$ denote the Lyapunov exponent of the attractor corresponding to a given θ. Thus $h_\varphi^{(k)}(\theta)=0$ for θ in the quasiperiodic range (gray regions of Fig. 6) and $h_\varphi^{(k)}(\theta)<0$ for θ in the periodic range (gaps in the gray regions). Since the attractor with irrational ω generates a uniform density in θ [see Eq. (5a)], we take the order-k RA to the Lyapunov exponent h_φ to be

$$\langle h_\varphi^{(k)}\rangle=\frac{1}{2\pi}\int_0^{2\pi} h_\varphi^{(k)}(\theta)\,d\theta. \tag{8}$$

For $\eta>0$, due to the existence of periodic components, $\langle h_\varphi^{(k)}\rangle$ is negative. As η increases for a given level k, the Lebesgue measure in θ for the periodic components increases, and hence $h_\varphi^{(k)}(\theta)$ becomes negative in a wider range in θ, as shown in Figs. 8(a) and 8(b) for level $k=6$. Thus, as η increases, $\langle h_\varphi^{(k)}\rangle$ decreases [see Fig. 8(c)].

In addition, we note that as the level k increases, the RA to the Lyapunov exponent h_φ converges rapidly to its quasiperiodic limit [represented by the solid line in Fig. 8(c)]. For comparison, the approximate analytic result for h_φ (i.e., $h_\varphi=-\eta^2/4$) is also given (see the dashed line). Consequently, for any nonzero η the attractor in the quasiperiodic limit has a Lyapunov exponent whose value decreases as η is increased.

We now discuss the strangeness of the attractor in the quasiperiodic limit for $\eta=0.3$. In the quasiperiodic case, we have seen (Fig. 3) that a typical trajectory seems to fill the whole torus densely, but, unlike the case of the regular quasiperiodic attractor, it appears to spend most of its time on a set of 1D strands. We identify these apparent 1D strands with the $k\to\infty$ limit of the main periodic component. Although, as k becomes larger, the Lebesgue measure of the quasiperiodic region approaches zero [Fig. 7(c)], these quasiperiodic regions become dense in θ. Since each quasiperiodic region fully covers the φ interval $[0,2\pi)$, the attractor is expected to occupy the entire θ-φ torus, and, hence, it is expected to have a box-counting dimension of 2.

III. HIGH DIMENSIONAL MAPS

A. Radial perturbations of the torus map

We now show that stability to perturbations applies, in addition, if the system is higher dimensional. In particular, we discuss the case of a three-dimensional system with an attracting invariant torus, and allow perturbations of the toroidal surface. Consider the following map on $\mathbf{R}^3$:

$$\theta_{n+1}=[\theta_n+\omega](\mathrm{mod}\,2\pi), \tag{9a}$$

$$\varphi_{n+1}=[\theta_n+\varphi_n+\eta\overline{P}(\theta_n,\varphi_n,r_n)](\mathrm{mod}\,2\pi), \tag{9b}$$

$$r_{n+1}=\lambda r_n+\rho Q(\theta_n,\varphi_n,r_n). \tag{9c}$$

Here θ and φ are coordinates on a torus embedded in $\mathbf{R}^3$, as in Fig. 1, and r is a coordinate transverse to the torus, with $r=0$ representing the unperturbed $(\lambda=\rho=0)$ torus. The parameters ω and η, and the dependence of $\overline{P}$ on θ and φ, have the same properties as for map (5), and Q is continuously differentiable and 2π periodic in θ and φ. When λ

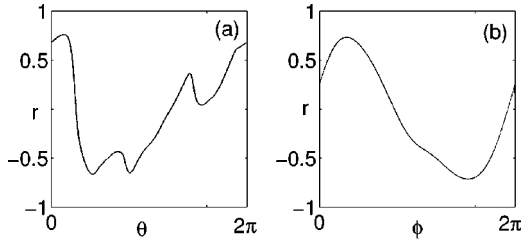

FIG. 9. Attractors in two-dimensional surfaces. (a) r vs θ at $\varphi=\pi$ surface and (b) r vs φ at $\theta=\pi$ with $\rho=0.5$, $\lambda=0.5$, and $\eta=0.3$ ($h_\varphi=-0.024$ and $h_r=-1.370$).

and ρ are small, Eq. (9) maps a neighborhood of the torus $r=0$ into itself, and when $\rho=0$ the torus $r=0$ is invariant and attracting. It then follows from classical results on the perturbation of invariant manifolds [18] that, for λ and ρ sufficiently small, the map (9) has a smooth attracting invariant manifold $r=f(\theta,\varphi)$ near the torus $r=0$. On this attractor, the map (9) reduces to a map of the form (5), with $P(\theta,\varphi)=\overline{P}[\theta,\varphi,f(\theta,\varphi)]$. Thus statements (i)-(v) above apply also to the attractor of the three-dimensional map (9).

The above arguments depend on the existence of a smooth invariant torus on which the attractor is located, and this is guaranteed if λ and ρ are sufficiently small. We now show numerical evidence for the existence of a smooth invariant torus for values of λ and ρ that are appreciable. We consider the example $\overline{P}(\theta,\varphi,r)=\sin\varphi$ and $Q(\theta,\varphi,r)=\sin(r+\varphi)$. We numerically obtain two-dimensional plots of intersections of the invariant torus with the surfaces $\varphi=\pi$ [Fig. 9(a)] and $\theta=\pi$ [Fig. 9(b)]. First consider the case $\varphi=\pi$. Our numerical technique is as follows. We choose an initial value $(\theta_0,\varphi_0=\pi)$ and obtain $(\theta_{-n},\varphi_{-n})$ by iterating Eqs. (9a) and (9b) backward n steps. Since $h_r\sim\ln\lambda<0$ (when $\rho\ll\lambda<1$), $r_{-n}\to\pm\infty$ as $n\to t^\infty$ if r_0 is not on the torus. In other words, if $r_{-n}=0$, then r_0 approaches the torus as $n\to t^\infty$. Thus, we choose $r_{-n}=0$ and iterate $(r_{-n},\theta_{-n},\varphi_{-n})$ forward ($n\gg1$) steps to $(r_0,\theta_0,\varphi_0=\pi)$. By varying θ_0, we obtain an approximation to the graph $r_0(\theta_0)$ of the torus intersection with $\varphi=\pi$. Similarly, choosing $(\theta_0=\pi,\varphi_0)$ and iterating the map (9) backward, and then forward, we can obtain an approximation $r_0(\varphi_0)$ to the equation of the torus intersection with $\theta=\pi$. (For our numerical experiments, we set $n=25$.) As shown in Fig. 9, a smooth invariant torus exists in the parameter region where ρ and λ are appreciable.

In Figs. 10(a) and 10(b) we show dimension computations for the map (9) with $\overline{P}(\theta,\varphi,r)=\sin(\varphi)$ and $Q(\theta,\varphi,r)=\sin(r+\varphi)$. [In this three-dimensional case we employ ε edge length cubes in (θ,φ,r)-space.] As for Fig. 4 we observe from Fig. 10 that the results are consistent with slow convergence to the predicted dimension values of 2 and 1 as the orbit length T is increased.

B. Map on a high-dimensional torus

In Sec. II. A we proved that Eq. (5) is topologically transitive. Here we show how this argument can be modified to higher dimensional maps that include $N>1$ quasiperiodic

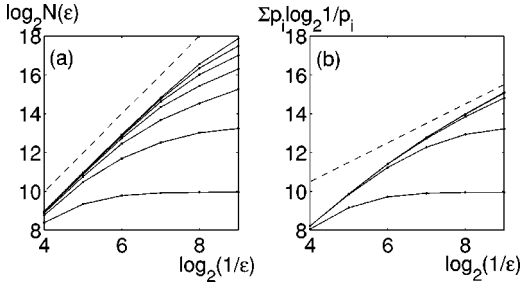

FIG. 10. Dimension computations for Eq. (9) with $\eta=0.3$, $\lambda=0.5$, $\rho=0.5$, $\omega=\pi(\sqrt{5}-1)$, $\overline{P}(\theta,\varphi)=\sin\varphi$, and $Q(\theta,\varphi,r)=\sin(r+\varphi)$. In (a) the dashed line has slope 2, while in (b) it has slope 1. In each graph, the curves from lowest to highest represent $T=10^3,10^4,\ldots,10^9$; in (b) the final four curves are virtually identical.

driving variables $\theta^{(1)}$, $\theta^{(2)}$, $\ldots$, $\theta^{(N)}$. For exposition we assume $N=2$, but the argument is virtually identical for all N.

In particular, we consider a map of the form

$$\theta^{(1)}_{n+1}=[\theta^{(1)}_n+\omega^{(1)}](\mathrm{mod}\,2\pi), \tag{10a}$$

$$\theta^{(2)}_{n+1}=[\theta^{(2)}_n+\omega^{(2)}](\mathrm{mod}\,2\pi), \tag{10b}$$

$$\varphi_{n+1}=[q^{(1)}\theta^{(1)}_n+q^{(2)}\theta^{(2)}_n+\varphi_n+\eta P(\theta^{(1)}_n,\theta^{(2)}_n,\varphi_n)](\mathrm{mod}\,2\pi), \tag{10c}$$

where $\omega^{(1)}$ and $\omega^{(2)}$ are incommensurate, $(q^{(1)},q^{(2)})$ is a pair of integers different from (0,0), and $P(\theta^{(1)},\theta^{(2)},\varphi)$ is continuous, differentiable, and 2π periodic in all of its arguments ($\theta^{(1)}$, $\theta^{(2)}$, and φ). We assume without loss of generality that $q^{(1)}\neq0$.

Let $R_a=\{(\theta^{(1)},\theta^{(2)}):\theta^{(1)}_a<\theta^{(1)}<(\theta^{(1)}_a+\delta_a)$ and $\theta^{(2)}_a<\theta^{(2)}<(\theta^{(2)}_a+\delta_a)\}$ and $R_b=\{(\theta^{(1)},\theta^{(2)}):\theta^{(1)}_b<\theta^{(1)}<(\theta^{(1)}_b+\delta_b)$ and $\theta^{(2)}_b<\theta^{(2)}<(\theta^{(2)}_b+\delta_b)\}$ be two arbitrary squares in the $\theta^{(1)}$-$\theta^{(2)}$ torus, and let $S_a=\{(\theta^{(1)},\theta^{(2)},\varphi):(\theta^{(1)},\theta^{(2)})\in R_a$ and $\varphi=\varphi_a\}$ and $S_b=\{(\theta^{(1)},\theta^{(2)},\varphi):(\theta^{(1)},\theta^{(2)})\in R_b$ and $\varphi=\varphi_b\}$ be a pair of square segments, where φ_a and φ_b are arbitrary. As before, we will show that there is a finite trajectory that begins on S_a and ends on S_b.

In this case, we proceed by iterating R_a forward until the union of its iterates covers all points $(\theta^{(1)},\pi)$ at least once (see Fig. 11). The number of iterates needed is finite. Then we select pieces of these iterates that single covers a thin strip $D_a=\{(\theta^{(1)},\theta^{(2)}):\pi\leqslant\theta^{(2)}\leqslant\pi+\varepsilon_a\}$ with rectangles of width ε_a. From the corresponding pieces of the corresponding iterates of S_a, we form the graph $\varphi=g_a(\theta^{(1)},\theta^{(2)})$ of a piecewise continuous function g_a defined on D_a. Similarly we form a graph $\varphi=g_b(\theta^{(1)},\theta^{(2)})$ on a strip D_b from pieces of backward iterates of $R_b\{\varphi_b\}$. As before, we will show that some forward iterate of the graph of g_a must intersect the graph of g_b.

Next, form the strip G_a by taking the graph of g_a and adding "connecting faces" at each of the d_a values of $\theta^{(1)}$ where g_a is discontinuous, so as to make G_a a contiguous strip. The construction of G_a is essentially as shown in Fig. 5(b), except that it now has some thickness in the $\theta^{(2)}$ direction (not shown). For each n, the nth iterate of G_a is also a contiguous strip that consists of the graph of a function with d_a discontinuities in the $\theta^{(1)}$ direction, together with d_a connecting faces, over a strip in the $\theta^{(1)}$-$\theta^{(2)}$ torus of width ε_a in

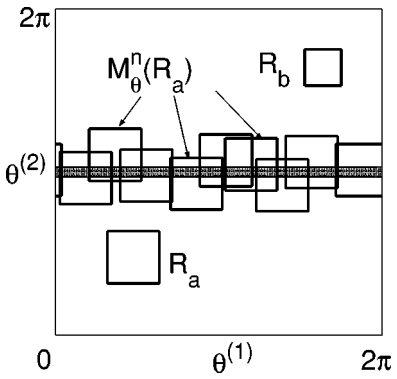

FIG. 11. Construction of the domain D_a (shaded region) of g_a.

the $\theta^{(2)}$ direction. Notice though that the strip moves a distance $\omega^{(2)}$ in the $\theta^{(2)}$ direction with each iteration. Define g_b and G_b similarly to g_a and G_a, but in terms of the backward iterates of S_b, and let d_b be the number of values of $\theta^{(1)}$ at which g_b is discontinuous.

As before, we can define the winding number of strips like G_a and G_b, representing the net number of times the strip wraps in the φ direction as $\theta^{(1)}$ increases from 0 to 2π. The winding number can be computed for any fixed value of $\theta^{(2)}$ and does not depend on that value. With each iteration of Eq. (10), the winding number of such a strip changes by $q^{(1)} \neq 0$. Therefore for n sufficiently large, the winding number of the nth iterate of G_a differs from the winding number of G_b by at least $d_a + d_b + 1$. Furthermore, by increasing n if necessary, we can ensure that the domains of these two strips intersect; that is, they have a common value of $\theta^{(2)}$. Then for that value of $\theta^{(2)}$, it follows as before that the nth iterate of the graph of g_a (without the d_a connecting faces of G_a) and the graph of g_b (without the d_b connecting faces of G_b) must intersect as claimed.

Our numerical experiments also give a sense of the above proof. In order to obtain two-dimensional plots, we count points when the trajectory passes through a thin slab of width $\delta \ll 1$ containing the $\theta^{(i)}$-φ surface. (For our experiments, the width of the slab is $\delta = 0.01$.) The results we obtain for the intersections of the attractors with the $\theta^{(2)} = \pi$ surface and the $\theta^{(1)} = \pi$ surface are qualitatively similar to the figure for the two-dimensional case (Fig. 3).

IV. CONCLUSION

In this paper we addressed the existence of robust strange nonchaotic attractors. We provided rigorous analysis for the two-dimensional map (5) in Sec. II A and for the $(N+1)$-dimensional maps of the form of Eq. (3) in Sec. III B. In particular, we have shown that the information dimension of the attractor for these maps is $D_1 = N$, while the box-counting dimension is $D_0 = N + 1$ [21]. In addition, we have used a rational approximation technique (Sec. II B) to investigate the dynamical origin of SNA's, as well as to gain additional understanding on why, in our $N = 1$ example, $D_1 = 1$ and $D_0 = 2$. In Sec. III A, we show that the stability to perturbations (robustness) continues to apply in systems [e.g., Eq. (9)] where there can be an attracting torus. We also carried out calculations to see how our rigorous dimension results are manifested numerically. Our results confirm the existence of SNA's as a generic phenomenon of quasiperiodically forced systems.

ACKNOWLEDGMENTS

S.-Y.K. thanks W. Lim for his help in the numerical work. This work was supported by the Korea Research Foundation (Grant No. KRF-2001-013-D00014), by the ONR (Physics), and by the NSF (DMS-0104087 and PHYS-0098632).

[1] C. Grebogi, E. Ott, S. Pelikan, and J.A. Yorke, Physica D **13**, 261 (1984).
[2] A. Bondeson, E. Ott, and T.M. Antonsen, Phys. Rev. Lett. **55**, 2103 (1985); F.J. Romeiras, A. Bondeson, E. Ott, T.M. Antonsen, and C. Grebogi, Physica D **26**, 277 (1987); Phys. Scr. **40**, 442 (1989).
[3] M. Ding, C. Grebogi, and E. Ott, Phys. Rev. A **39**, 2593 (1989).
[4] F.J. Romeiras and E. Ott, Phys. Rev. A **35**, 4404 (1987).
[5] J.A. Ketoja and I.I. Satija, Physica D **109**, 70 (1997).
[6] W.L. Ditto, M.L. Spano, H.T. Savage, S.N. Rauseo, J. Heagy, and E. Ott, Phys. Rev. Lett. **65**, 533 (1990).
[7] J.F. Heagy and S.M. Hammel, Physica D **70**, 140 (1994).
[8] U. Feudel, J. Kurths, and A.S. Pikovsky, Physica D **88**, 176 (1995).
[9] T. Nishikawa and K. Kaneko, Phys. Rev. E **54**, 6114 (1996).
[10] T. Yalcinkaya and Y.C. Lai, Phys. Rev. Lett. **77**, 5039 (1996).
[11] A. Prasad, V. Mehra, and R. Ramaswamy, Phys. Rev. Lett. **79**, 4127 (1997).
[12] A. Witt, U. Feudel, and A.S. Pikovsky, Physica D **109**, 180 (1997).
[13] B.R. Hunt and E. Ott, Phys. Rev. Lett. **87**, 254101 (2001).
[14] M. Ding, C. Grebogi, and E. Ott, Phys. Lett. A **137**, 167 (1989).
[15] For an introduction of the RA approach, see J.M. Greene, J. Math. Phys. **20**, 1183 (1979); R.S. MacKay, Physica D **7**, 283 (1983).
[16] H. Furstenberg, Am. J. Math. **83**, 573 (1961).
[17] F. Ledrappier, Commun. Math. Phys. **81**, 229 (1981).
[18] See, for example, A. Katok and B. Hasselblatt, *Introduction to the Modern Theory of Dynamical Systems* (Cambridge University Press, Cambridge, England, 1995).
[19] J. Stark, Physica D **109**, 163 (1997); R. Sturman and J. Stark, Nonlinearity **13**, 113 (2000).
[20] G. Keller, Fundam. Math. **151**, 139 (1996).
[21] Chaotic attractors with D_0 equal to the dimension of the phase space and $D_1 < D_0$ are not uncommon. Some examples are Ch. Dellago *et al.*, Phys. Rev. E **52**, 4817 (1995); Ya.G. Sinai, Russ. Math. Surveys **27**, 21 (1972). We believe, however, that in these cases, $(D_0 - D_1)$ is relatively small compared to one.